*Articles*

# Human Integrin αv$\beta$5: Homology Modeling and Ligand Binding

Luciana Marinelli,[‡] Kay-E. Gottschalk,[§] Axel Meyer,[†] Ettore Novellino,[‡] and Horst Kessler*[,†]

*Institut für Organische Chemie und Biochemie, Technische Universität München, Lichtenbergstrasse 4, D-85747 Garching, Germany, Department of Biological Chemistry, Weizmann Institute of Science, Herzl St. 1, Rehovot, 76100 Israel, and Dipartimento di Chimica Farmaceutica e Tossicologica, Università di Napoli "Federico II", Via D. Montesano, 49-80131 Napoli, Italy*

*Received December 18, 2003*

The recently reported crystal structures of the extracellular domains of the αv$\beta$3 integrin in its unligated state and in complex with the peptide *cyclo*(-RGDf[NMe]V-) have dramatically increased our understanding of ligand binding to integrins. Nonetheless, ligand selectivity toward different integrin subtypes is still a challenging problem complicated by the fact that 3D structures of most of the integrin subtypes remain unknown. In this study, a three-dimensional model for the human αv$\beta$5 integrin was obtained using homology modeling based on the crystal coordinates of αv$\beta$3 in its bound conformation as template. The modeled receptor was refined using energy minimization and molecular dynamics simulations in explicit solvent. The refined αv$\beta$5 model was used to explore the interactions between this integrin and αv$\beta$3/αv$\beta$5 dual and αv$\beta$3-selective ligands in the attempt to provide a preliminary rationalization, at the molecular level, of ligand selectivity toward the two αv integrins. It was found that, in the RGD binding site of the αv$\beta$5 receptor, a partial "roof" composed mainly of the SDL residues Tyr179 and Lys180 is present and hampers the binding of compounds containing bulky substituents in the proximity of the carboxylate group. This study provides a testable hypothesis for αv integrins subtype ligand binding selectivity, in line with both mutagenesis data and SARs studies.

## Introduction

The concept that tumor growth and its spread are dependent on the formation of new blood vessels has sparked an interest in identifying protein targets, which inhibit the formation of vessels and which are amenable to regulatory interactions with small-molecule drugs.[1] The angiogenic process depends on vascular endothelial cell proliferation, migration, and invasion. A family of adhesion receptors, the integrins, are involved in these processes.[2] Until now, attention has been paid to the role of αv integrins in angiogenesis, especially the αv$\beta$3.[3] Interaction of this receptor with monoclonal antibodies or low-molecular-weight ligands[4] inhibits blood-vessels formation in a variety of in vivo models.[5] It has also been shown that the related αv$\beta$5 integrin is involved in angiogenesis.[6] Nowadays, it is a widely shared opinion that neovascular disease in different tissues may induce two distinct integrin-mediated pathways: one induced by FGF2 and mediated by αv$\beta$3 and another induced mainly by VEGF and mediated by αv$\beta$5.[7] The biological relevance of these different pathways is still unknown. Perhaps, vascular remodeling in distinct organs depends on the particular growth factor and/or adhesive proteins contained within the specific extracellular matrix. Indeed, $\beta$3 integrin-deficient mice have normal brain and gut vessel development, while αv integrin-deficient mice have defective brain and gut blood vessels.[8] This strongly implicates another αv integrin, potentially αv$\beta$5, in brain and gut neovascularization. Therefore, selective and dual αv$\beta$3/αv$\beta$5 ligands both represent an interesting and novel class of angiogenesis and tumor-growth inhibitors.[9] Small molecule αv integrin ligands are currently being evaluated in phase I and II clinical trials for patients with late-stage cancer, e.g. cilengitide = c(-RGDfNMeVal-).[4,5]

Structurally, the integrins are heterodimeric glycoproteins composed of two noncovalently associated integral membrane subunits.[10] Nineteen α and eight $\beta$ subunits have been identified, which assemble into more than twenty-four different heterodimers. The most common integrin binding sequence is the Arg-Gly-Asp (RGD) motif, found within their matrix ligands.[11] However, different integrins recognize diverse RGD-containing proteins differently. It has been demonstrated that selectivity between the αv$\beta$3 and αIIb$\beta$3 can be achieved mainly by conformational control of the RGD sequence in the ligand.[12] Up to now, a large number of RGD-mimetic compounds have been identified as potent and often subtype-selective integrin ligands.[13]

One of the major determinants of ligand binding specificity between the integrin receptors is the variable subunit composition of this class of proteins. Integrins with the same α subunit, such as αv$\beta$3 and αv$\beta$5, as

* To whom correspondence should be addressed. Tel: +49-89-289 13300. Fax: +49-89-289 13210. E-mail: kessler@ch.tum.de.
† Technische Universität München.
§ Weizmann Institute of Science
‡ Dipartimento di Chimica Farmaceutica e Tossicologica, Università "Federico II" di Napoli.

10.1021/jm030635j CCC: $27.50 
Published on Web 07/10/2004

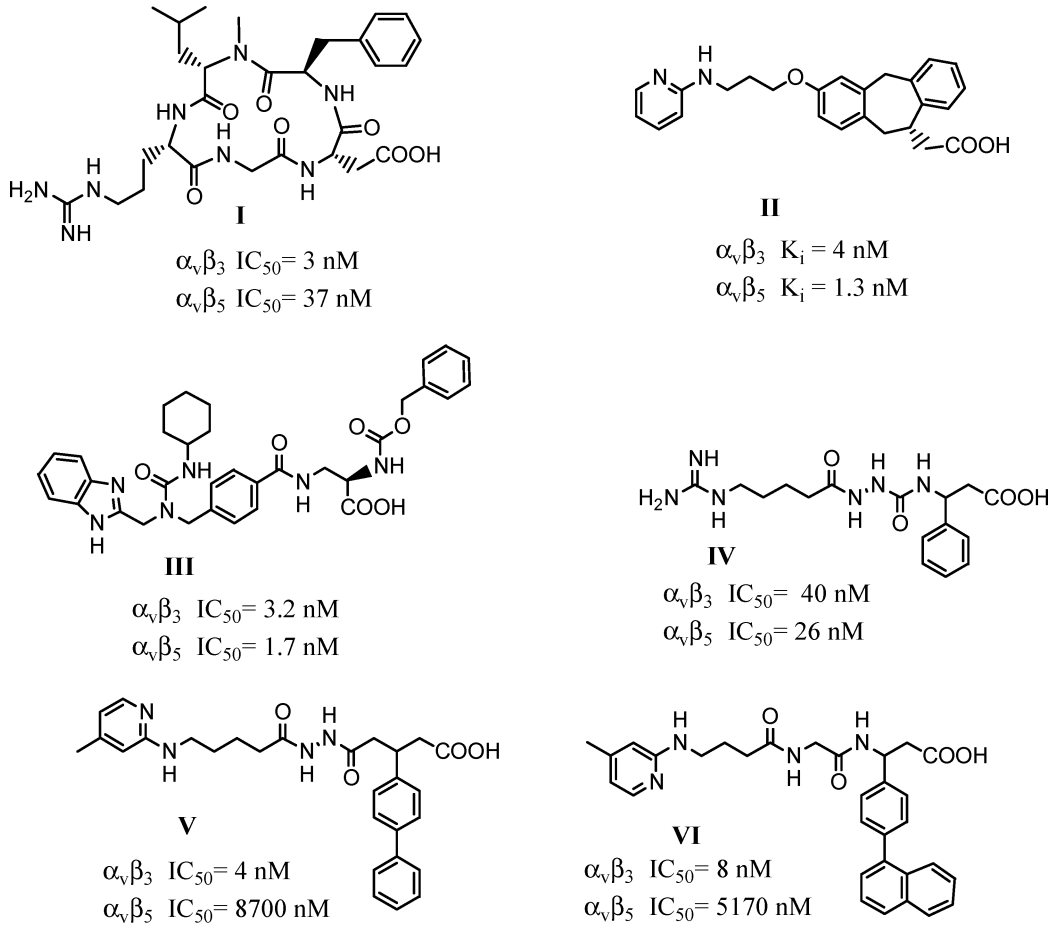


**Figure 1.** Structures of the docked ligands.

well as integrins with the same $\beta$ subunit, for example $\alpha5\beta1$ and $\alpha v\beta1$, have different ligand binding specificities. Hence, in the case of αv integrins, it is evident that the nonconserved residues in the $\beta$ subunits account for the different ligand specificity. The RGD binding surface in the $\alpha v\beta3$ integrin is composed by the $\beta$-propeller domain in the α subunit and the I-like domain in the $\beta$ subunit. Within the I-like domain, each $\beta$ subunit contains a long loop, which is divergent among all the $\beta$ chains (residues 159−188[1] (The $\beta3$ sequence numbering was retrieved from the PBD database. Each residue in the $\beta5$ subunit has been numbered according to the $\beta3$ subunit used as template.) in $\beta3$). The importance of this region for the natural ligand selectivity between the $\alpha v\beta3$ and the $\alpha v\beta5$ integrins was demonstrated by the construction of $\beta3/\beta5$ chimeras.[14] Within this loop, Takagi et al. identified a short disulfide-linked sequence, (CYDMKTTC in the case of $\beta3$) responsible for the $\alpha v\beta3$ ligands preference.[15] Therefore, this loop is commonly known as Specificity Determining Loop (SDL).

The recently determined X-ray crystal structure[16] of the extracellular domains of $\alpha v\beta3$ in complex with *cyclo*(-RGDf[NMe]V-), "cilengitide",[4] has shed new light on mechanisms of integrin−ligand binding. The ligand was found to bind in a groove between the $\beta$-propeller and the I-like domain with one of the carboxylate oxygens of the Asp side chain coordinating directly to a $Mn^{2+}$ ion in the MIDAS site. The Arg side chain bound entirely to loops in the $\beta$-propeller. Only small conformational changes (restricted to the I-like domain and the $\beta$-propeller) were observed between the ligand-occupied and ligand-free states,[16,17] leading to considerable controversy about the molecular basis of activation.[18−20]

This X-ray structure is a snapshot of different conformations that represent diverse activity levels of the receptor and therefore is not sufficient to understand the complete mechanism of cell adhesion as well as inside-out or outside-in signaling which involves dramatic motions and reorganization of the integrin subunits together with their binding molecules. The role of transmembrane helix−helix interaction remains controversial.[19]

Starting from the $\alpha v\beta3$−*cyclo*(-RGDf[NMe]V-) complex, structural models for the interactions of known small ligands with the $\alpha v\beta3$ integrin receptor were presented.[20] This approach led to a structural understanding of ligand binding to this integrin. Previous and recent studies of homology modeling and ligands docking led to proposals of $\alpha4\beta1/\alpha4\beta7$ and $\alpha v\beta3/\alpha IIb\beta3$ ligand binding selectivity.[21]

Here, the $\alpha v\beta5$ receptor was investigated by means of a combined approach of homology modeling and ligand−receptor docking. We have constructed the headgroup of the $\alpha v\beta5$ integrin, which contains all the regions responsible for ligand recognition and binding. As regards the docking studies, $\alpha v\beta3/\alpha v\beta5$- and $\alpha v\beta3$-selective ligands were used, which are potential drug candidates and have been thoroughly characterized experimentally (Figure 1).

The results of this study will be presented in terms of comparative analyses between the two receptors. The

```
                    159                                                188
ITB3_HUMAN          KPVSPYMYISPPEALENPC--YDMKTTCLPMF
ITB3_MOUSE          KPVSPYMYISPPQAIKNPC--YNMKNACLPMF
ITB5_HUMAN          KDISPFSYTAP-RYQTNPCIGYKLFPNCVPSF
ITB5_PAPCY          KDISPFSYTAP-RYQTNPCIGYKLFPNCVPSF
ITB5_MOUSE          KDISPFSYTAP-RYQTNPCIGYKLFPNCVPSF
ITB6_HUMAN          KPVSPFVKTTP-EEIANPCS--SIPYFCLPTF
ITB6_CAVPO          KPVSPFMKTTP-EEIANPCS--SIPYICLPTF
ITB6_MOUSE          KPVSPFMKTTP-EEITNPCS--SIPYFCLPTF
ITB1_FELCA          KTVMPYISTTP-AKLRNPCT--S-EQNCTSPF
ITB1_BOVIN          KTVMPYISTTP-AKLRNPCT--N-EQNCTSPF
ITB1_HUMAN          KTVMPYISTTP-AKLRNPCT--S-EQNCTTPF
ITB1_RAT            KTVMPYISTTP-AKLRNPCT--S-EQNCTSPF
ITB1_MOUSE          KTVMPYISTTP-AKLRNPCT--S-EQNCTSPF
ITB1_CHICK          KTVMPYISTTP-AKLRNPCT--G-DQNCTSPF
ITB7_HUMAN          KTVLPFVSTVP-SKLRHPCP--TRLERCQSPF
ITB7_MOUSE          KTVLPFVSTVP-SKLHHPCP--SRLERCQPPF
ITB2_PIG            KTVLPFVNTHP-EKLRNPCP--NKEKECQAPF
ITB2_BOVIN          KTVLPFVNTHP-EKLRNPCP--NKEKECQPPF
ITB2_HUMAN          KTVLPFVNTHP-DKLRNPCP--NKEKECQPPF
ITB2_MOUSE          KTVLPFVNTHP-EKLRNPCP--NKEKACQPPF
ITB8_HUMAN          KTVSPYISIHP-ERIHNQCS--DYNLDCMPPH
ITB8_RABIT          KTVSPYISIHP-ERIHNQCS--DYNLDCMPPH
ITB4_RAT            KVSVPQTDMRP-EKLKEPWP------NSDPPF
ITB4_HUMAN          KVSVPQTDMRP-EKLKEPWP------NSDPPF
                    *   *     *          .          . . .
```

**Figure 2.** Multiple sequence alignment of integrin $\beta$ subunits, corresponding to the $\beta_3$ residues 159−188, obtained with ClustalW. The aligned sequences correspond to the SDL region. Blue stars (*) represent the fully conserved residues, while the blue point (·) represents the conservation of weak groups.

comparison was performed at three different levels. First, the two receptors were compared in their primary sequence. Second, the respective RGD binding sites were analyzed in their structural context. Finally, the two receptors have been compared in their interaction modes with $\alpha v\beta 3/\alpha v\beta 5$ dual- and $\alpha v\beta 3$-selective ligands.

At all three levels of complexity, this study offers an insight into the $\alpha v\beta 5$ receptor structure and into its interaction mode with potential drugs and provides a possible mechanism behind $\alpha v$ integrins subtype ligand binding selectivity.

## Results and Discussion

**Sequences Analysis.** A multiple sequence alignment was performed, utilizing evolutionary information of all $\beta$-subtypes in different organisms. The sequence-alignment of the integrin $\beta$ subunits demonstrated that the majority of the differences between the $\beta 3$ and $\beta 5$ subunits can be observed at the region comprising residues 159−188[1] in $\beta 3$ (SDL). Figures 2 and 3 show that within the SDL the residues preceding the NPC sequence display a certain level of homology. The two disulfide-bonded segments, on the other hand, are very different in the sequence and in the number of residues. The $\beta 5$ subunit has a two-residue insertion with respect to the $\beta 3$, and most of the other residues are not highly conserved. Nevertheless, certain key residues, which are probably crucial for the structural integrity of the loop, are highly conserved in the integrin family. The two prolines, ($\beta 3$)-Pro163 and ($\beta 3$)-Pro169, are among the most conserved residues in the whole sequence. Another proline, ($\beta 3$)-Pro176, which is flanked by Asn and Cys forming the motif NPC, is highly conserved among the $\beta$ subunits. It is worth noting that all three Pro are involved in $\beta$ turns and are probably responsible for the U-shape of the SDL. The cystein in the NPC motif ($\beta 3$)-Cys177 and the ($\beta 3$)-Cys184 are always conserved with the exception of integrin $\beta 4$, which is known to be less similar to all other integrin $\beta$ subtypes. The two Cys form a disulfide bridge within the loop, reducing considerably the accessible conformational space of the disulfide-linked sequence. It is most likely that this disulfide bond is conserved in all the members of the family with the exception of $\beta 4$-containing integrins and plays an important role from a structural point of view. Takagi et al.[15] showed that swapping this short part of the sequence between $\beta 1$ and $\beta 3$ also swaps their natural ligand preference. The recently determined X-ray structure shows that this part of the sequence is located at the RGD ligand binding site.[16]

For the remaining part, the RGD binding site is highly conserved between the two $\alpha v$ integrins as shown in Figure 4. In particular, ($\beta 3$)-Arg214, ($\beta 3$)-Asn215, ($\beta 3$)-Arg216 (sequence RNR) are conserved among all type of $\alpha v\beta 3$ and $\alpha v\beta 5$ integrins and are a unique feature of these types of receptors. In a previous docking study using small ligands and $\alpha v\beta 3$ as receptor, we found that all three residues participate in the ligands binding. Differently, ($\beta 3$))-Tyr 122, which was found to interact with the Phe side chain of *cyclo*(-RGDf[NMe]V-) (see Figure 4), is replaced by the smaller Leu122 in the $\alpha v\beta 5$ receptor. This residue is characteristic for the $\beta 5$ subunit. In all the other $\beta$ subunits a Tyr is present with the exception of $\beta 6$ and $\beta 4$, which exhibit an Ala and an Asn residue, respectively. All residues surrounding the metals at the MIDAS, ADMIDAS, and LIMBS region are highly conserved with the exception of ($\beta 3$)-Ala252, which is replaced by an Asp residue. The latter residue probably coordinates the metal ion at the MIDAS region in the $\beta 5$ subunit. The divalent cations are essential for integrin functions, ranging from stabilizing the integrin structure to enhancing or suppressing its interaction with physiologic ligands (reviewed in 22). The importance of the conservation of the metal coordinating residues is demonstrated by the fact that nonconservative mutations within or nearby the propeller's metal coordinating loops cause loss of integrin expression.[23]

Two more replacements far from the ligand binding site are present and are illustrated in Figure 4. The ($\beta 3$)-Glu312 and the ($\beta 3$)-Ser334 are substituted in $\beta 5$ by a Lys and an Asp, respectively.

The sequence analysis of the $\alpha\beta$ interface demonstrates that the $\beta 5$ residues at interface with $\alpha v$ subunit are conserved to a very large extent with respect to $\beta 3$. As shown in Figure 5, the majority of changed residues are located in the SDL region (($\beta 3$))-Ile167, ($\beta 3$))-Ser168, ($\beta 3$))-Pro170, ($\beta 3$))-Glu171). It has been observed that the SDL deletion does not affect the heterodimer formation by several integrin subtypes including $\alpha v\beta 3$.[24]

The remaining part of the I-like domain, which is responsible for the majority of contacts with the $\alpha v$ subunit, is highly conserved. Two interesting substitutions are present: the ($\beta 3$)-Lys253, which in the X-ray complex forms a hydrogen bond with the ($\alpha v$)-Asp219, is replaced by a Val residue in $\beta 5$ and the ($\beta 3$)-Arg261 is replaced by a Lys. The $\alpha v\beta 3$ X-ray structure shows that the ($\beta 3$)-Arg 261 inserts into the central hole of the $\beta$-propeller domain (Figure 5) and is caged into place by two concentric rings of predominantly aromatic residues. Cation$-\pi$ binding between the positive charged Arg and the surrounding aromatic residues is likely to be conserved with the Lys replacement. It was previously speculated that a small change in ($\beta 3$)-Arg261 side

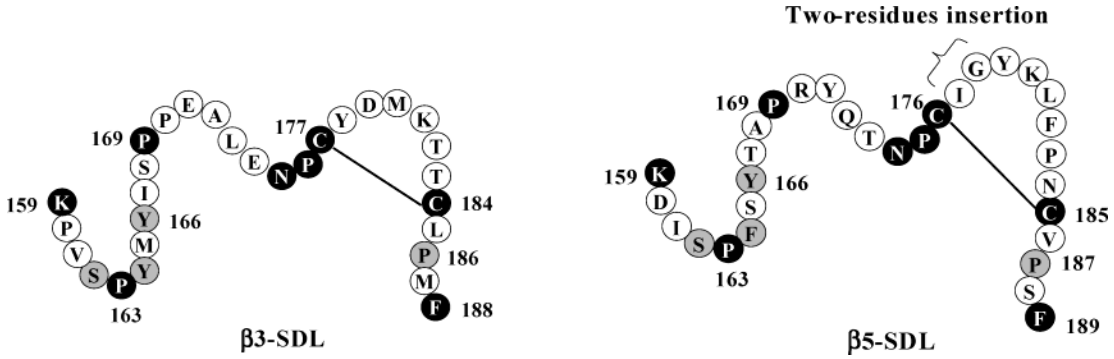


**Figure 3.** Schematic representation of the αvβ3 and αvβ5 SDL region. Residues are denoted by their one-letter code. Black circles denote highly conserved residues in the integrin family. Gray circles represent conservation of amino acids between αvβ3 and αvβ5. Disulfide bridges between C177 and C184 and C176 and C185 are shown as lines connecting these cysteines.

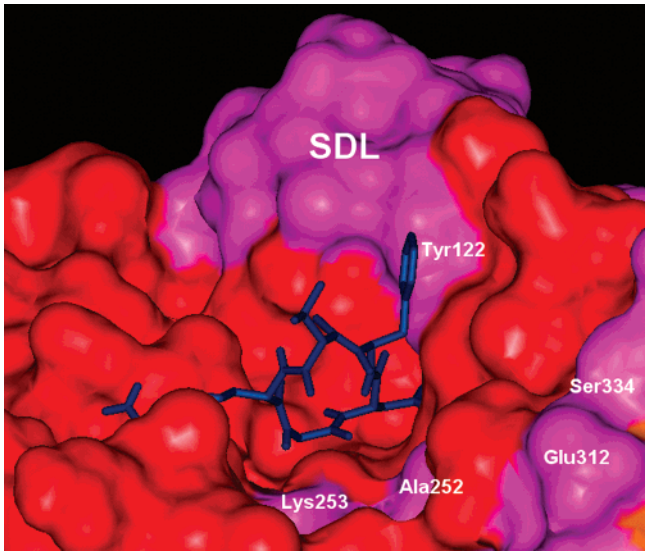


**Figure 4.** Sequence conservation at the RGD binding site between the αvβ3 and αvβ5 receptors mapped onto the molecular surface of the human αvβ3 complex. Regions of sequence identity are colored in red, while the nonconserved regions are labeled and colored in magenta. The *cyclo*(-RGDf[NMe]V-) ligand is represented in blue color.

chain orientation could modulate the stability of αvβ3 interface due to attractive or repulsive amide-aromatic interaction.[17]

**Modeling of αvβ5 Receptor and General Features of the Model.** Under physiological conditions, the integrins are thought to interconvert between different conformations that represent diverse activity levels.

It is unlikely that these conformational transitions would occur spontaneously during a molecular dynamics simulation using current state-of-the-art approaches. Consequently, the αvβ5 integrin has been modeled directly in its bound conformation using as template the X-ray structure of the αvβ3 integrin in complex with the *cyclo*(-RGDf[NMe]V-) ligand. It has to be mentioned that small quaternary changes are observed when the unliganded and liganded structures of αvβ3 are superimposed. However, due to the fact that the ligand was diffused into existing αvβ3 crystals it is probable that the observed changes represent a minimalist view of the changes taking place during the macromolecular ligand binding. For the purpose of docking small synthetic ligands, the αvβ3 -*cyclo*(-RGDf[NMe]V-) represent an ideal template.

Due to the high percentage of sequence identity at the αβ interface between the αvβ5 receptor and the used template together with the fact that the two integrins bind common small ligands, it has been assumed that the αv and β5 subunit assemble in a similar manner as found for αvβ3. Hence, the β5 subunit were manually merged with the αv subunit and with *cyclo*(-RGDf[NMe]V-) ligand, which possess high affinity for both αv integrins, according to the template. Special care was paid in the modeling of SDL due to its importance and its low degree of conservation.

An attempt to model this loop structure was made by generating possible structures that satisfy the spatial requirements of the disulphide bond between (β5)-Cys176 and (β5)-Cys185 and, at the same time, occupy approximately the same region in the 3D model structure as in αvβ3 integrin complex. A 600 ps MD simulation of the SDL in the presence of the *cyclo*(-RGDf[NMe]V-) ligand and in the context of the entire integrin head was performed (see Methods). A superimposition of β5 SDL conformations extracted from the last 250 ps of the MD simulationwas is shown in Figure 6.

The SDL region, closer to the αv subunit (from (β5)-Lys159 to (β5)-Arg170), did not change remarkably during the MD simulation. In both receptors, the SDL residues$^{167-170}$ contacted a flat region composed mainly by residues from (αv)-Gln120 to (αv)-Arg122. This is in line with the hypothesis from Takagi et al. that for the SDL an α subunit-specific conformation exists.[24] The side chain orientation of (β5)-Lys180 hardly changed during the simulation; it seems held in place by both ionic and hydrophobic interactions with (β5)-Tyr179. Remarkable movements of (β5)-Lys180 side chain were also hampered by the opposite (β5)-Lys125 side chains. Due to these considerations, the β5 SDL can be considered as relatively conformationally constrained.

The stability of the SDL during the MD simulation gave the opportunity to use the average of the production run for the subsequent analysis and docking experiments. The presence of the small (β5)-Leu122 allows the reorientation of the (β5)-Tyr179 and (β5)-Lys180 to form a partial "roof" above the RGD binding site. In the αvβ3 receptor a Tyr is present instead of a Leu, and an Asp and a Met are in place of (β5)-Tyr179 and the (β5)-Lys125, respectively. Consequently, the

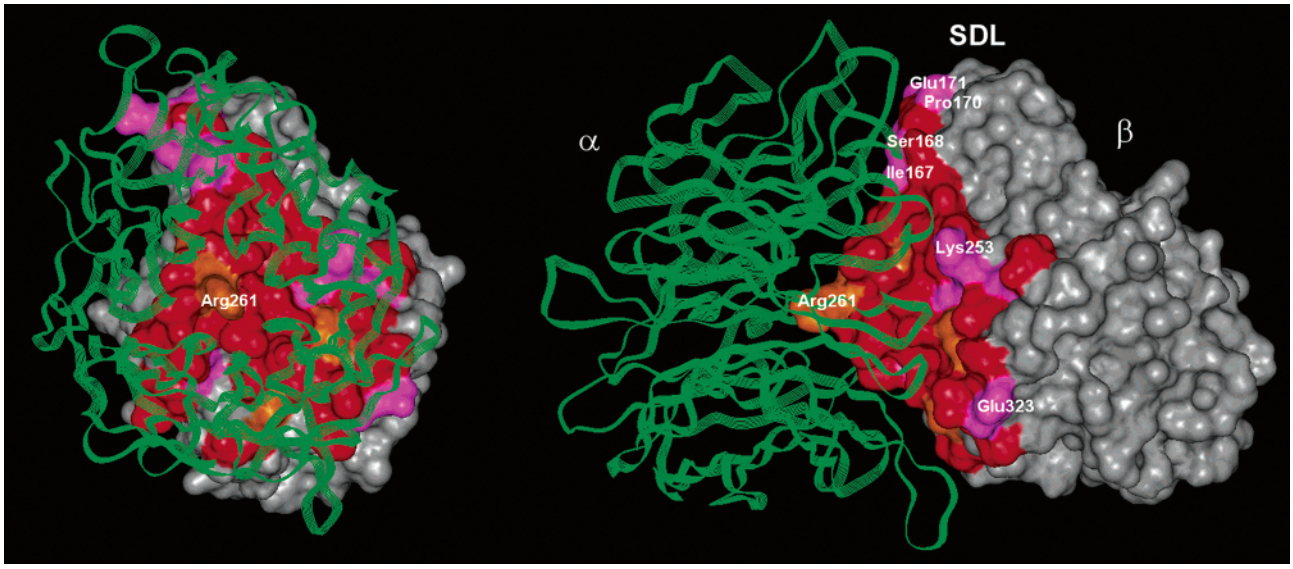


**Figure 5.** Sequence conservation at the α−*β* interface between the αv*β*3 and αv*β*5 receptors mapped onto the human αv*β*3 complex. The αv subunit is represented as green ribbon while the *β*3 subunit as Connolly surface. On the right side, a front side view is presented, and on the left side a rotated 90° view, which show the Arg261 protruding off-center into the propeller's channel. Regions of sequence identity are colored in red, semiconserved regions are in orange while the nonconserved regions are labeled and colored in magenta.

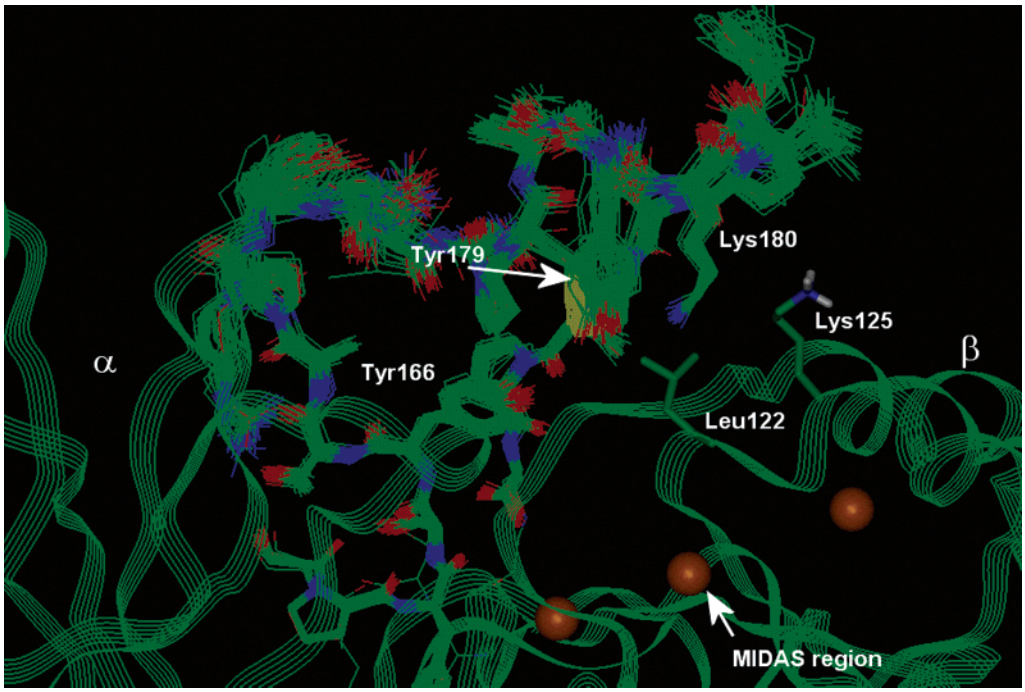


**Figure 6.** Superimposition of *β*5 SDL conformations extracted from the last 250 ps of the MD simulation. The SDL is represented as line mode and colored by atom type. The disulfide bond between (*β*5)-Cys176 and (*β*5)-Cys185 is visible in yellow. The remaining part of the *β*-subunit and the α subunit are represented as green ribbon drawing. Three metal ions are visible at MIDAS, ADMIDAS, and LIMBS region as orange spheres.

αv*β*3 RGD binding site is broader in that region with respect to αv*β*5.

As expected from the high homology and from the low number of insertion/deletions in the alignment, the overall topology of the template protein was conserved and is described elsewhere[10,16,17] (Figure 7). The stereochemical quality of the resulting model was checked with the program PROCHECK. The majority of the residues of the modeled complex occupy the most favored region of the Ramachandran plot, and the other residues occupied additional allowed regions. After molecular dynamics, 75.6% of the residues were in the most favored region, 21.1% in additional allowed region, 2.9% in the generously allowed region, and only the 0.3% were in disallowed region. It has to be mentioned that, in the final stage of the complex refinement, both the ligand and the protein side-chain atoms in the binding site were allowed to relax. The αv*β*5 binding site defined for *cyclo*(-RGDf[NMe]V-) ligand was then utilized for the remaining ligands.

**Ligand Binding Analysis.** There have been very few endogenous ligands identified to bind the αv*β*5 receptor, and all known αv*β*5 ligands also bind to the αv*β*3 integrin. The latter is supposed to have a more

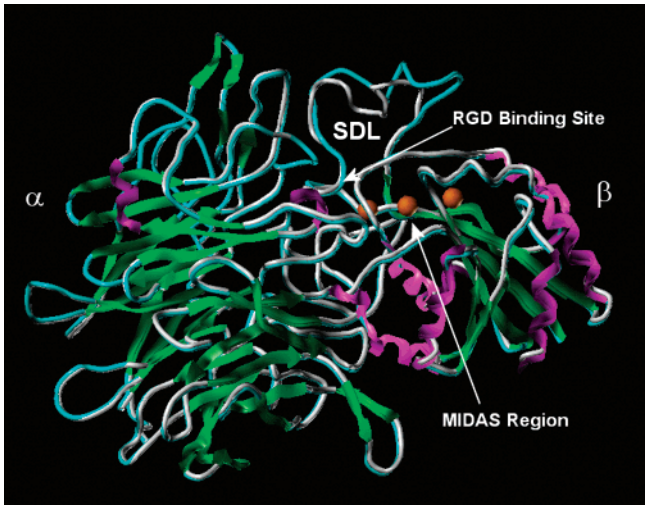


**Figure 7.** Three-dimensional structure of extracellular domains of αvβ5 integrin overlapped on the template. The superposition were performed considering all the backbone atoms. α-Helices and β strands are colored in magenta and green, respectively. αvβ5 loops are shown in cyan, while αvβ3 loops are shown in gray. The RGD binding site and the MIDAS region are indicated by white arrows. As shown in figure, the major difference between the two complexes resides in the conformation of the specificity determining loop (SDL).

relaxed ligand binding specificity as it binds to at least six more endogenous ligands than αvβ5.

The refined αvβ5 model was used to explore the the interactions between this integrin and αvβ3/αvβ5 dual and αvβ3-selective ligands in the attempt to provide a preliminary rationalization, at the molecular level, of ligand selectivity toward the two αv integrins. The chemical structures of the docked ligands[4,9,13g,25] together with the activities toward the two αv receptors are shown in Figure 1.

**Docking of αvβ3/αvβ5 Dual Ligands to αvβ3 and αvβ5 Receptors.** Compounds **I**, **II**, **III**, **IV** were manually positioned in the receptors binding site and then ran up to 50 docking procedures per ligand. For each compound, only one or two clusters of binding modes were found to be in line with the experimental data. For instance, a frequent binding mode shows the ligand carboxylic acid interacts with (β3/β5)-Arg214/5. This solution was rejected as it was postulated early on that the $Ca^{2+}$ ion at the MIDAS region interacts with the aspartic acid of RGD peptides. Such an interaction was recently observed for the *cyclo*(-RGDf[NMe]V-) in the X-ray complex, and its importance has subsequently been discussed by Arnaout et al.[26]

The selected binding modes were common for all the docked ligands and revealed a consistent set of recurring interactions in line with the experimental data (Figures 8-9). In both receptors, the ligands insert into a crevice between the propeller and the βA domain on the integrin head. The Asp and Arg mimetic side chains point to opposite directions allowing the carboxylate group in the ligand to coordinate the $Ca^{2+}$ in the MIDAS region and the guanidinium(-like) moiety to bind the (αv)-Asp150 end/or (αv)-Asp218. The involvement of these two Asp in the ligand binding is in accordance with the mutagenesis data,[27] cross-linking studies,[28] and X-ray structure, all of which indicate (αv)-Asp150 and (αv)-Asp218 are fundamental residues in the interaction with the RDG ligands.

The coordination of the metal ion is complemented by favorable contacts with the backbone amide proton of (β5)-Asn216. In the case of **III**, which possesses an aromatic moiety on the Arg-mimicking side chain, a π-stacking interaction with the (αv)-Tyr178 side chain was observed. This is in line with the mutagenesis data, which indicates the importance of (αv)-Tyr 178 in ligand binding.[29] For those ligands which possess a hydrogen bond donor group in the proximity of the carboxylate moiety, a hydrogen bond with the backbone CO of (β5)-Arg217 was found (see binding modes of **I**, **III**, **IV**).

Compound **I**, which was synthesized in our lab and biologically tested by Merck KGaA (Darmstadt, Germany), turned out to be 10 orders of magnitude more active on the αvβ3 integrin. In the αvβ3 binding, the Phe side chain stabilizes the complex through a T-shape interaction with the (β3)-Tyr122 (16). According to that, SAR studies by our lab, together with molecular docking, showed that substitution of D-Phe by D-Trp or βNal increases the binding affinity due to an enlargement of the hydrophobic interaction with the (β3)-Tyr122.[12,16,20] Differently, in the αvβ5 integrin, due to the replacement of (β3)-Tyr122 by the (β5)-Leu122, such favorable interaction cannot occur (Figure 8a) leading probably to a slight loss of activity on αvβ5 ($IC_{50}$=37 nM) with respect to αvβ3 ($IC_{50}$ = 3 nM).

In the case of **II**, two possible binding modes were observed due to the flexibility of the arginine mimetic side chain. In both binding modes, the NH within the aminopyridine ring donates a hydrogen bond to the (αv)-Asp218. In the more populated binding mode (17 structures out of 50) represented by the compound colored in green in Figure 8b, the arginine mimetic group inserts into the narrow groove at the top of the propeller domain (region of (αv)-Asp150, (αv)-Asp218). In the second most populated binding mode (8 structure out of 50) represented by the compound colored in orange, the aminopyridine ring binds in the region of (αv)-Asp218, (αv)−(αv)-Arg248, and (β5)-Val254. In both binding modes, a π-stacking interaction between one phenyl ring in the dibenzocycloheptane and the (αv)-Tyr178 side chain is present (the distance between the centroids of the two rings is 5.7). Docking of **II** in αvβ3 receptor revealed a strong preference for one binding mode, which corresponds to the more populated in the αvβ5. The second binding mode found within αvβ5 seems not to be possible in the αvβ3 receptor due to the substitution of (β5)-Val254 with (β3)-Lys253, whose long side chain hampers an allocation of the aminopyridine ring similar to that found within the αvβ5 receptor.

Compound **III** is a particular interesting ligand having high affinity for all three types of integrins involved in the angiogenesis process (αvβ3:3.2 nM, αvβ5: 1.7 nM, α5β1: 421 nM) but only poor affinity for αIIbβ3 (1294 nM). The flexibility of the branch near the carboxylate group allows the phenyl ring to make a T-shaped interaction with the (β5)-Tyr166 side chain and to avoid a steric clash with the β5 SDL (β5)-Tyr179 (β5)-Lys180 (Figure 9a). Docking of **III** into the αvβ3 integrin results in an analogous binding mode. This finding is in line with the similar activity found for compound **III** on the two receptors.

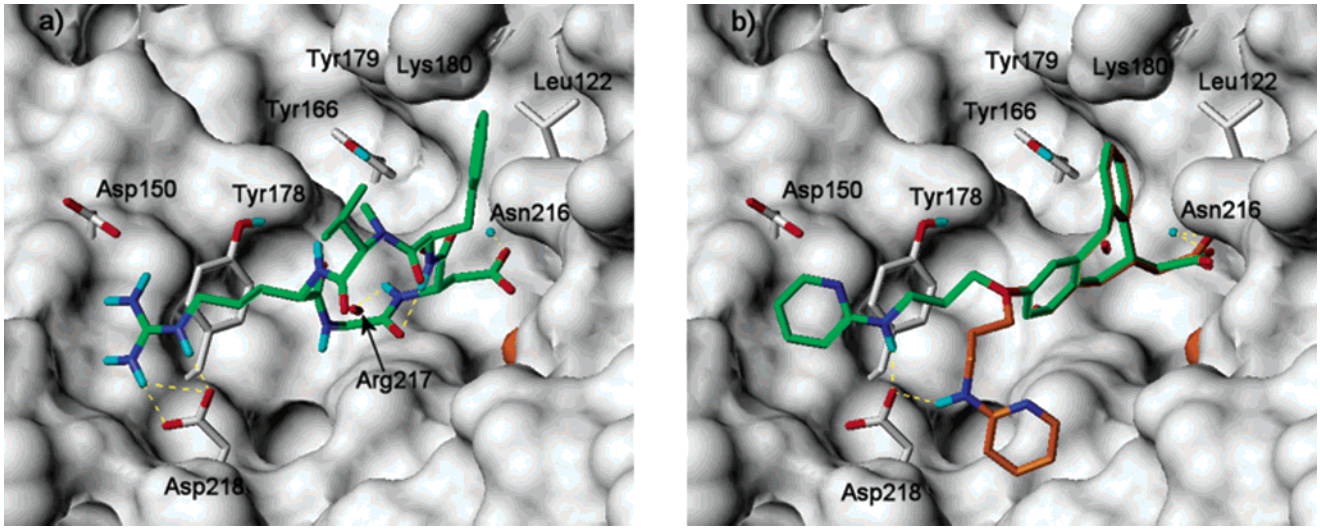


**Figure 8.** (a) Binding mode of compound **I** within the αv$\beta$5 RGD binding site represented as Connolly surface. Ligand carbons are colored in green, while receptor surface in light gray. The metal ion at the MIDAS region is represented as orange sphere. Some residues in the receptor were removed for clarity. (b) Binding mode of compound **II** within the αv$\beta$5 RGD binding site. Two possible binding modes were showed. The most populated (see text) is in green, the other in orange.

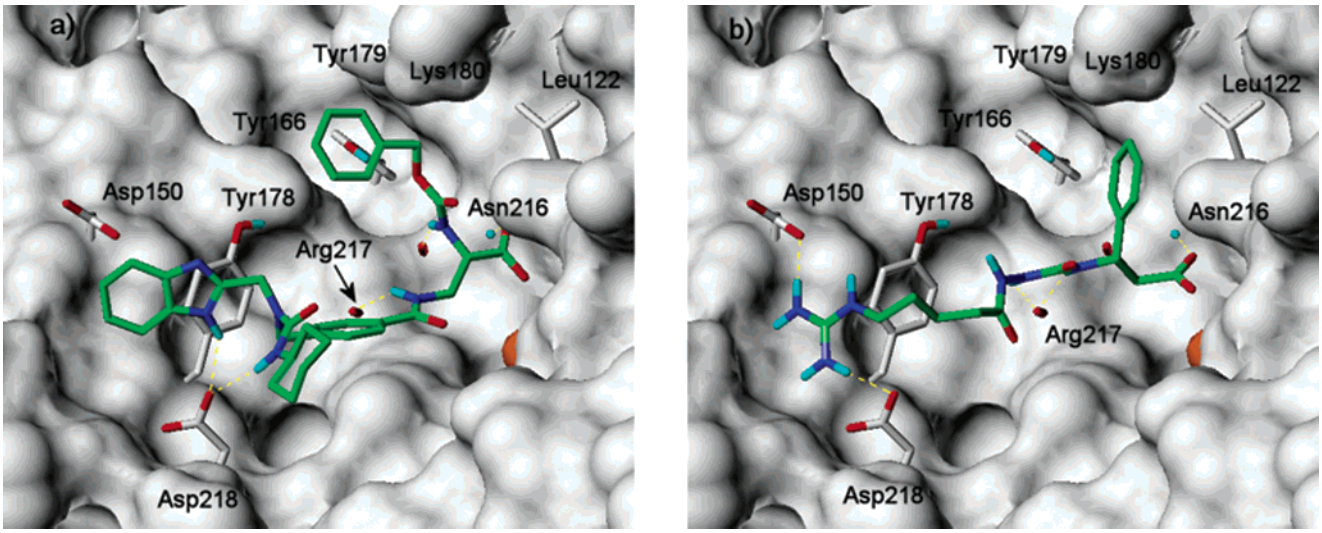


**Figure 9.** Binding mode of compound **III** (a) and **IV** (b) within the αv$\beta$5 RGD binding site.

Regarding compound **IV**, the most populated binding mode (13 structures out of 50) presents the phenyl ring oriented perpendicular to the plain of the molecule, pointing toward the SDL residues ($\beta$5)-Lys180 and ($\beta$5)-Tyr179 represented in Figure 9b as Connolly surface. The distance between the centroid of the ligand phenyl ring and Nζ of the ($\beta$5)-Lys180 is 5.6 Å, while with the centroid of the ($\beta$5)-Tyr179 ring is 7.3 Å. The found binding mode perfectly explains the productive insertion of the diacylhydrazine moiety in the proximity of the carboxylate group; it mimics the Asp backbone amide proton of **I** in its interaction with the ($\beta$3)-Arg216. Docking of **IV** in the αv$\beta$3 integrin gave perfectly comparable results.

Therefore, according to our model, the following interactions govern the αv$\beta$5 ligands recognition process: (i) coordination of $Ca^{2+}$ ion at the MIDAS from the carboxylate moiety of the ligand; (ii) a salt bridge between the (αv)-Asp218 or the (αv)-Asp150 and the guanidine(-like) moiety of the bound ligand; (iii) a hydrogen bond donated by one ligand NH to the carbonyl oxygen of ($\beta$5)-Arg217 backbone (iv) $\pi$-stacking interaction from one aromatic ring in the ligand and (αv)-Tyr178.

Taking into account the previously reported docking studies on αv$\beta$3 receptor,[20] it can be observed that conserved regions of the αv integrins receptors (i.e. (αv)-Asp150, (αv)-Asp218, (αv)-Tyr178, ($\beta$3/5)-Asn215/6, ($\beta$3/5)-Arg216/7, $Ca^{2+}$ in the MIDAS region) bind the common chemical component of the dual ligands (guanidine(-like) moiety, aromatic group, hydrogen bond donor group, carboxylate moiety). The proposed ligands binding modes, where conserved regions of the receptors bind conserved motif of the ligands, find similarities with that of many other receptors such as opioid, dopamine, or chemokine receptors.[30]

Nonetheless, selectivity between the two αv receptors through the incorporation of a phenyl ring or naphthyl at the 4-position of the phenyl ring of **IV** (**V** and **VI**) was achieved successfully.[13g] SARs relative to **IV** and to its analogues clearly indicate that the region, in which the phenyl group of **IV** allocates, is narrower in αv$\beta$5 with respect to αv$\beta$3. The high affinity and particularly the high selectivity with which **V** and **VI** bind to the

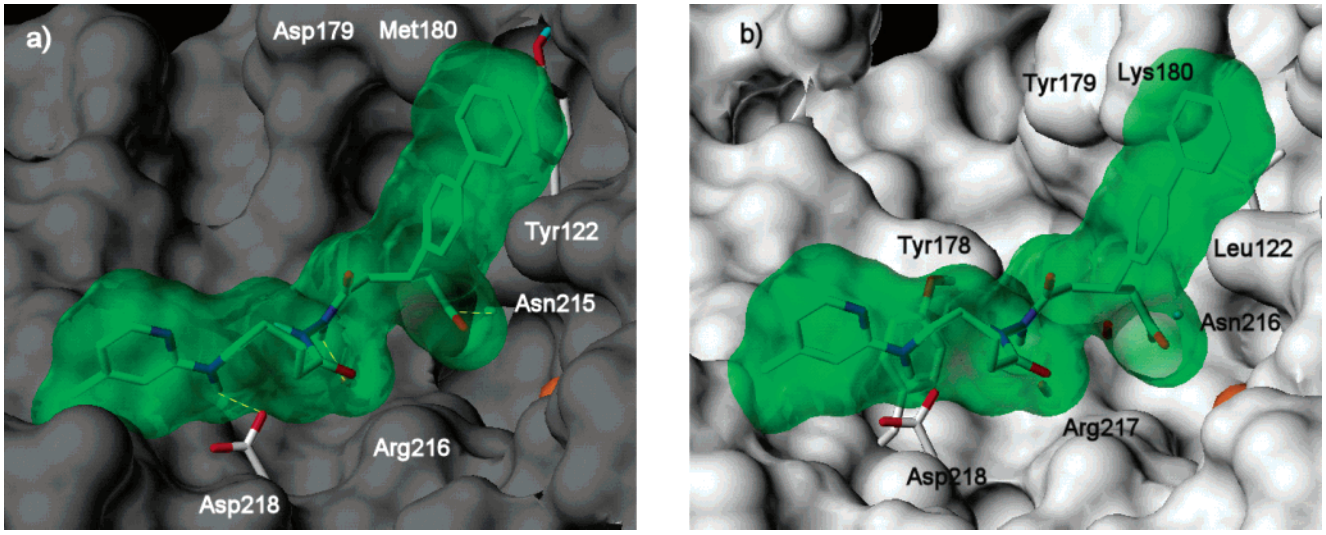


**Figure 10.** (a) Binding mode of compound **V** within the αvβ3 RGD binding site. The ligand is represented as green transparent Connolly surface, while the αvβ3 binding site is represented as dark gray Connolly surface to highlight the complementarity between the ligand and the αvβ3 receptor binding site. (b) Binding mode of compound **V** within the αvβ5 RGD binding site. An evident clash between the biphenyl moiety in the ligand and the receptor surface ((β5)-Lys180) is visible.

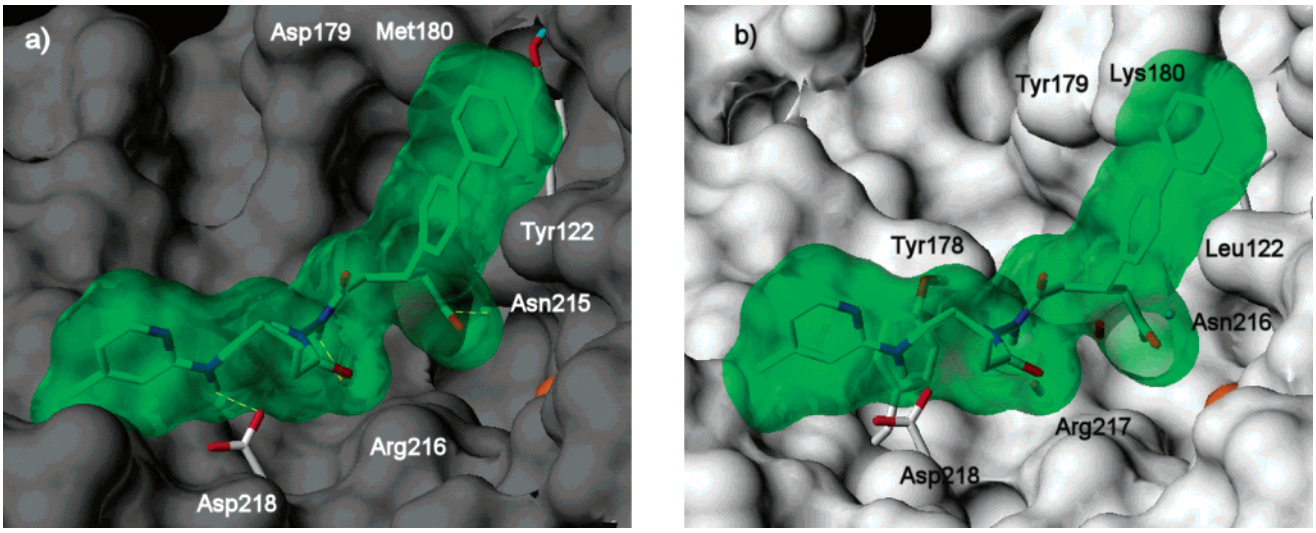


**Figure 11.** (a) Binding mode of compound **VI** within the αvβ3 RGD binding site. (b) Binding mode of compound **VI** within the αvβ5 RGD binding site. An evident clash between the naphthyl moiety in the ligand and the receptor surface ((β5)-Lys180 and (β5)-Tyr179) is visible.

αvβ3 integrin raises the important issue of which molecular features underlie the differences in their interaction with αvβ3 versus αvβ5 integrins. Hence, these two αvβ3-selective compounds were docked first in αvβ3 and then in αvβ5 receptor in the attempt to find an explanation of the ligands binding selectivity.

**Docking of αvβ3-Selective Ligands to αvβ3 and to αvβ5 Receptor.** Docking of compounds **V** and **VI** in the αvβ3 receptor resulted in comparable binding modes where all the interactions, which are thought vital for the binding, are conserved (Figures 10a and 11a). As expected, in compound **V**, the biphenyl moiety is placed in such a way that a T-shape interaction with (β3)-Tyr122 (represented as sticks in Figure 10a) occurs. One amide proton of the diacylhydrazino moiety donates a hydrogen bond to the backbone CO of the (β3)-Arg216.

The αvβ3-selective ligands were automatically docked in the αvβ5 receptor. Docking of **V** and **VI** resulted in several orientations in which the ligand carboxylate group did not coordinate the metal ion at the MIDAS region. However, most of these structures lay above the RGD binding site without making appreciable interaction with the αvβ5 binding surface. These results suggest that the binding site made up by the αv and β5 subunits cannot accommodate such ligands. Manual docking of compounds **V** and **VI** in an orientation similar to that found using the αvβ3 as receptor, reveals that a steric clash between the ligands and the SDL (β5)-Lys180 and (β5)-Tyr179 residues would occur (Figures 10b and 11b). In these compounds, all the possible orientations of the aromatic moietys were considered, resulting always in a steric overlap with the β5 surface. A different orientation of the biphenyl moiety of **V** to avoid the clash would result in a loss of the ligand interactions with the αvβ5 key residues. A superimposition of the two αv integrins (Figure 12) shows that the region, in which the biphenyl moiety allocates is narrower in the αvβ5 receptor with respect to αvβ3 due to the presence of (β5)-Lys180 and (β5)-Tyr179 as compared to (β3)-Asp179 and (β3)-Met180. (β5)-Tyr179,

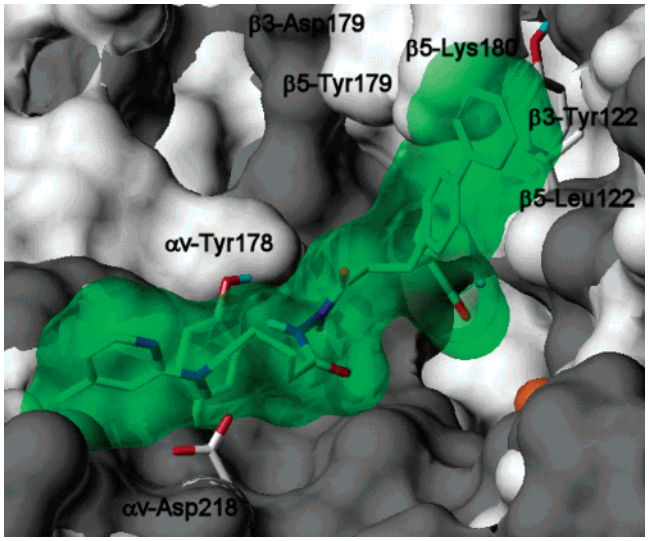


**Figure 12.** Superposition of αv$\beta$3 and αv$\beta$5 receptors, both represented as Connolly surfaces (dark and light gray respectively), within **V** bound to the αv$\beta$3 integrin.

especially, is bulkier than ($\beta$3)-Asp179. Notable is also the different charge contribution (Lys for $\beta$5 and Asp for $\beta$3), which might have an additional effect on ligand binding. As mentioned above, the $\beta$5-SDL is two amino acids longer with respect to that of $\beta$3 and the corresponding residues which rise above the RGD binding site are bulkier in $\beta$5 SDL leading to the formation of a partial "roof". Given the flexibility of amino acids side chains, one might argue that the ($\beta$5)-Lys180 could rearrange itself in a such a way to allow the allocation of **V** and **VI** phenyl rings. This effect can hardly occur since ($\beta$5)-Lys180 is constrained in its mobility by the equally charges residue ($\beta$5)-Lys125 and by the adjacent ($\beta$5)-Tyr179.

The two amino acids ($\beta$5)-Tyr179 and ($\beta$5)-Lys180, which seem to play a role in the αv$\beta$5 ligand binding selectivity are part of the disulfide bound sequence, a highly divergent segment within the long SDL, which is known to have a substantial impact on the ligand selection of integrins.[14−15]

Our hypothesis would explain the SARs studies, which indicate the difficulty of αv$\beta$5 integrin to allocate bulky systems in proximity to the carboxylate groups as in the case of **V** and **VI**.[13g]

Hence, the presented three-dimensional models for a number of complexes of dual and selective ligands with both the αv$\beta$3 and αv$\beta$5 receptors are consistent with a large body of experimental data and lead us to propose experimentally testable hypotheses for the molecular bases of ligand subtype selectivity. As more data are available to better characterize the details of interactions between different integrins and their ligands, these issues will be resolved more definitively.

This study was limited to docking small ligands which contain or mimic the smallest recognition unit (RGD) of many types of integrin, but natural ligands are significantly larger, structurally more diverse and often multivalent. Indeed, experiments using chimeras of αv$\beta$3 and αv$\beta$5 and using Fab-9 and fibrinogen as ligands, both of which have a binding preference for αv$\beta$3, suggest that the complete ligand binding specificity is achieved through the contact between ligands with several discontinuous domains of the $\beta$ subunit.

## Conclusion

Based on the X-ray structure of the human αv$\beta$3 integrin bound to the RGD-containing peptide *cyclo*(-RGDf[NMe]V-), a 3D structural model of αv$\beta$5 receptor was built. In an attempt to provide a preliminary rationalization, at the molecular level, of ligand selectivity toward the two αv integrins, the latter were carefully compared in their primary sequence, in their RGD binding site features and in their interaction with different ligands. Here three-dimensional models are presented for a number of ligands complexes with αv$\beta$3 and αv$\beta$5 receptors that are consistent with a large body of experimental data. Our docking results, when combined with mutagenesis data and cross linking studies, suggest a common binding mode for the dual RGD-mimetic ligands on the two αv receptors.

According to our theoretical αv$\beta$5 model, the two integrins differ especially in the region above the MIDAS due to the diversity of the SDL. A partial "roof" composed mainly from the SDL residues ($\beta$5)-Tyr179 and ($\beta$5)-Lys180 is present in the αv$\beta$5 receptor and hampers the binding of compounds containing bulky substituents in the proximity of the carboxylate group.

## Experimental Methods

**Sequence Alignment.** The alignment of the integrin $\beta$1−$\beta$8 sequences corresponding to $\beta$3 residues 109−353 (integrin head) was obtained by means of the CLUSTALW package applying the default parameters.[31] The few gaps in the alignment fell mainly in the region corresponding to the SDL (Figure 2). Therefore, the other parts of the protein can be considered as being sequentially and structurally conserved.

**Model Building.** The program MODELLER (version 6.2)[32] was used to build 20 full-atom models of human $\beta$5 subunit according to the comparative protein modeling method. The template used was the X-ray structure of the αv$\beta$3 integrin in complex with the *cyclo*(-RGDf[NMe]V-) ligand (PDB entry code = 1L5G). The human $\beta$3 and $\beta$5 subunits are highly homologous, sharing 65% identity in the construct used. The modeling procedure is conceptually similar to that used in the determination of protein structures from NMR-derived restraints. The restraints, distances and dihedral angles, are extracted from the template structure. Additionally, stereochemical restraints such as bond length and bond angle preferences obtained from the molecular mechanics force field of CHARMM-22 are used together with statistical preferences of dihedral angles and nonbonded atomic distances obtained from a representative set of all known protein structures. The model is then calculated through cycles of geometry optimization and molecular dynamics simulation.

Twenty models were built and ranked using the MODELLER objective function, which is highly efficient in ranking different models calculated from the same alignment.[32] The backbone atoms of the predicted models overlapped well and differed mainly in the conformation of the SDL region (residues 159−188 in $\beta$3). The highest ranking model of the $\beta$5 subunit was subjected to further refinement in this region. Although the SDL is significantly less conserved than the rest of the protein, certain key residues, which are crucial for the structural integrity of the loop, are highly conserved among the integrins family (Figure 3). Hence, these key residues were taken as anchor points for the SDL refinement.

**Dynamics Simulations.** To assess the preferred conformation of the SDL in the presence of the ligand and in the context of the entire integrin headpiece, a 600 ps molecular dynamics simulation of the complex was carried out in explicit solvent. For this purpose the $\beta$5 subunit was manually merged with

the αv and with the *cyclo*(-RGDf[NMe]V-) ligand, which possess high affinity for both integrins (*β*3 and *β*5), taking as template the αv*β*3- *cyclo*(-RGDf[NMe]V-) complex. The $Mn^{2+}$ were replaced by $Ca^{2+}$ ions. The residues Arg, Lys, Glu, and Asp were taken in their charged form, while all His residues were considered neutral by default, resulting in a total charge of −9*e*. To make the system electroneutral, nine sodium counterions were added. With the aid of VEGA (vs 1.5.0) program,[33] the ions were placed around the integrin headgroup, where the electrostatic energy achieved the smallest values. The complex was then soaked with a 5 Å water layer. The calculations were carried out with the DISCOVER module of the INSIGHTII program using CVFF force field.[34] A multiple-step procedure was used. The complex was energetically minimized with 3000 steps of a steepest descent minimization, followed by 5000 steps of conjugate gradient minimization to adjust the water molecules and the counterions locally and to eliminate any residual geometrical strain, keeping the heavy atoms of the headgroup fixed. The minimized solvated system was used as initial structure for the subsequent molecular dynamics (MD) simulation. MD calculation was begun with an initial and equilibration stage (100 ps), followed by a production run (500 ps). In the equilibration stage, energy minimization of the protein side chains were achieved employing 3000 steps of steepest descent. Subsequently, the system was heated gradually starting from 10 to 300 K in 1 ps steps. The system was then equilibrated with temperature bath coupling (300 K) applying a tethering force on the loop backbone starting from 100 kcal/$Å^{-2}$ and decreasing to 0 kcal/$Å^{-2}$, the rest of the protein was kept fixed. A cutoff of 13 Å was used for nonbonded interactions. Coordinates and energies were saved every 5 ps yielding 120 structures.

The average structure was calculated over the 100 structures of the production run and was energy-minimized using 3000 steps of a steepest descent minimization keeping the backbone atoms constrained. The stereochemical quality of the final structure was analyzed using the program PROCHECK.[35]

**Molecular Docking.** Docking of ligands **I**−**VI** to αv*β*5 integrin was carried out using the AutoDock program package version 3.0.5.[36] The LGA algorithm, as implemented in the AutoDock program, was used applying a protocol with a maximum number of 1.5 × 106 energy evaluations, a mutation rate of 0.01, a crossover rate of 0.80, and an elitism value of 1. For the local search, the pseudo-Solis and Wets algorithm was applied using a maximum of 300 interactions per local search. Fifty independent docking runs were carried out for each ligand. Results differing by less than 1.5 Å in positional root-mean-square deviation (rmsd) were clustered together and represented by the result with the most favorable free energy of binding. The obtained complexes were energetically minimized using 3000 steps of steepest descent algorithm, permitting only the ligand and the side chain atoms of the protein within a radius of 5 Å around the ligand to relax. The geometry optimization was carried out employing the DISCOVER program with the CVFF force field.

**Ligand Setup.** The structures of the ligands were generated from the standard fragment library of the SYBYL software version 6.9 (37). Geometry optimizations were achieved with the SYBYL/MAXIMIN2 minimizer by applying the BFGS (Broyden, Fletcher, Goldfarb and Shannon)[38] algorithm with a convergence criterion of 0.001 kcal/mol and employing the TRIPOS force field.[39] Partial atomic charges were assigned using Gasteiger and Marsili formalism as implemented in the SYBYL package.[40] In case of **I**, the backbone in its bound conformation, as found in the αv*β*3 X-ray complex, was held fixed while the side chain dihedral angles were free to rotate. As regards the remaining ligands, all the relevant torsion angles were treated as flexible during the docking process thus allowing a search of the conformational space. In the case of compound **IV** and **V**, the Cambridge Structural Database (CSD)[41] was searched to investigate the conformational preference of the diacylhydrazine moiety. Since the torsion angle C−N−N−C was mostly found to be −90°, which is also in accordance with ab initio studies,[42] the geometry of this fragment was held fixed during the calculations. The organic compounds were docked in the S conformation which is well-known to be the most active isomer. Compound **II** was docked with the dibenzocycloheptane ring in the equatorial conformation since it was found as preferred conformation over the axial one in the binding to the αv*β*3 receptor.[20]

**Protein Setup.** The protein structure was set up for docking as follows: the unpolar hydrogens were removed, and Kollman united-atom partial charges were assigned. Solvation parameters were added to the final protein file using the ADDSOL utility of the AutoDock program. The grid maps were calculated with AutoGrid. The grids were chosen to be large enough to include a significant part of the protein around the binding site. In all cases, we used grid maps with 61 × 61 × 61 points with a grid-point spacing of 0.375 Å. The αv*β*3 crystal structure in complex with the *cyclo*(-RGDf[NMe]V-) was superimposed on the αv*β*5 model, and the center of the grid was set to be coincident with the mass center of the ligand in the crystal complex.

**Acknowledgment.** The authors thank Professor Arthur J. Olson for the donation of the Autodock 3.0.5 program. Special thanks go to Alessandro Pedretti and Giulio Vistoli for the donation of the VEGA 1.5.0 program. Financial support by the Fonds der Chemischen Industrie is acknowledged. K.E.G. is supported by a Minerva Fellowship.

## Abbreviations

MIDAS, metal-ion-dependent adhesion site; ADMIDAS, adjacent to metal-ion-dependent adhesion site; LIMBS, ligand-induced metal binding site.

## References

(1) (a) Brower, V. Tumor angiogenesis − new drugs on the block. *Nat. Biotechnol.* **1999**, *17*, 963−968. (b) Carmeliet, P.; Jain, R. K. Angiogenesis in Cancer and other Disease. *Nature* **2000**, *407*, 249−257. (c) Jain, R. K. Molecular regulation of vessel maturation. *Nat. Med.* **2003**, *9*, 685−693. (d) Marx, J. A Boost for Tumor Starvation. *Science* **2003**, *301*, 452−453.

(2) (a) Hynes, R. O. Integrins: Versatility, Modulation, and Signaling in Cell Adhesion. *Cell* **1992**, *69*, 11−25. (b) Hynes, R. O.; Bader, B. L.; Hodivala-Dilke, K. Integrins in Vascular Development. *Braz. J. Med. Biol. Res.* **1999**, *32*, 501−510. (c) Ruegg, C.; Dormond, O.; Foletti, A. Suppression of tumor angiogenesis through the inhibition of integrin function and signaling in endothelial cells: which side to target? *Endothelium* **2002**, *9*, 151−160. (d) Kim, S.; Bakre, M.; Yin, H.; Varner, J. A. Inhibition of endothelial cell survival and angiogenesis by protein kinase A. *J. Clin. Invest.* **2002**, *110*, 933−941. (e) Hynes, R. O. A reevaluation of integrins as regulators of angiogenesis. *Nature Medicine* **2002**, *8*, 918−921. (f) Mousa, S. A. Anti-integrin as novel drug-discovery targets: potential therapeutic and diagnostic implications. *Curr. Opin. Chem. Biol.* **2002**, *6*, 534−541

(3) (a) Brooks, P. C.; Clark, R. A.; Cheresh, D. A. Requirement of Vascular integrin αv*β*3 for angiogenesis. *Science* **1994**, *264*, 569−571. (b) Eliceiri, B. P.; Cheresh, D. A. Role of alpha v integrins during angiogenesis. *Cancer J.* **2000**, *13*, 245−249.

(4) Dechantsreiter, M. A.; Planker, E.; Mathä, B.; Lohof, E.; Hölzemann, G.; Jonczyk, A.; Goodman, S. L.; Kessler, H. *N*-Methylated Cyclic RGD Peptides as Highly Active and Selective αv*β*3 Integrin Antagonists. *J. Med. Chem.* **1999**, *42*, 3033−3040.

(5) Burke, P. A.; DeNardo, S. J.; Miers, L. A.; Lamborn, K. R.; Matzku, S.; DeNardo, G. L. Cilengitide Targeting of avb3 Integrin Receptor Synergizes with Radioimmunotherapy to Increase Efficacy and Apoptosis in Breast Cancer Xenografts. *Cancer Res.* **2002**, *62*, 4263−4272.

(6) (a) Smith, J. W.; Vesta, D. J.; Irwin, S. V.; Burke, T. A.; Cheresh, D. A. Purification and functional characterization of integrin alpha v beta 5. An adhesion receptor for vitronectin. *J. Biol. Chem.* **1990**, *265*, 11008−11013. (b) Friedlander, M.; Theesfeld, C. L.; Sugita, M.; Fruttinger, M.; Thomas, M. A.; Chang, S.; Cheresh, D. A. Involvement of Integrins αv*β*3 and αv*β*5 in Ocular Neovascular diseases. *Proc. Natl. Acad. Sci.* **1996**, *93*, 9764−9769.

(7) Friedlander, M.; Brooks, P. C.; Shaffer, R. W.; Kincaid, C. M.; Varner, J. A.; Cheresh, D. A. Definition of two angiogenic pathways by distinct alpha v integrins. *Science* **1995**, *270*, 1500−2.

(8) (a) Bader, B. L.; Rayburn, H.; Crowley, D.; Hynes, R. O. Extensive vasculogenesis, angiogenesis, and organogenesis precede lethality in mice lacking all alpha v integrins. *Cell* **1998**, *95*, 507−519. (b) Hodivala-Dilke, K. M.; McHugh, K. P.; Tsakiris, D. A.; Rayburn, H.; Crowley, D.; Ullman-Cullere, M.; Ross, F. P.; Coller, B. S.; Teitelbaum, S.; Hynes, R. O. $\beta_3$-integrin-deficient mice are a model for Glanzmann thrombasthenia showing placental defects and reduced survival. *J. Clin. Invest.* **1999**, *103*, 229−238.

(9) Kumar, C. C.; Malkowski, M.; Yin, Z.; Tanghetti, E.; Yaremko, B.; Nechuta, T.; Varner, J.; Liu, M.; Smith, E. M.; Neustadt, B.; Presta, M.; Armstrong, L. Inhibition of angiogenesis and tumor growth by SCH221153, a dual $\alpha v\beta 3$ and $\alpha v\beta 5$ integrin receptor antagonist. *Cancer Res.* **2001**, *61*, 2232−2238.

(10) (a) Humphries, M. J. Integrin structure. *Biochem. Soc. Trans.* **2000**, *28*, 311−339. (b) Hynes, R. O. Integrins: bidirectional, allosteric signaling machines. *Cell* **2002**, *110*, 673−687.

(11) (a) Ruoslahti, E.; Pierschbacher, M. D. New perspectives in cell adhesion: RGD and integrins. *Science* **1987**, *238*, 491−497. (b) D'Souza, S. E.; Ginsberg, M. H.; Plow, E. F. Arginyl-Glycyl-Aspartic acid (RGD) a cell adhesion motif. *Trends Biochem. Sci.* **1991**, *16*, 246−250.

(12) (a) Aumailley, M.; Gurrath, M.; Müller, G.; Calvete, J.; Timpl, R.; Kessler, H. Arg-Gly-Asp constrained within cyclic pentapeptides. Strong and selective inhibitors of cell adhesion to vitronectin and laminin fragment P1. *FEBS Lett.* **1991**, *291*, 50−54. (b) Müller, G.; Gurrath, M.; Kessler, H.; Timpl, R. Dynamic Forcing, a Method for Evaluating Activity and Selectivity Profiles of RGD (Arg-Gly-Asp) Peptides. *Angew. Chem., Int. Ed. Engl.* **1992**, *31*, 326−328. (c) Gurrath, M.; Müller, G.; Kessler, H.; Aumailley, M.; Timpl, R. Conformation/activity studies of rationally designed potent anti-adhesive RGD peptides, *Eur. J. Biochem.* **1992**, *210*, 911−921. (d) Peishoff, C. E.; Ali, F. E.; Bean, J. W.; Calvo, R.; D'Ambrosio, C. A.; Eggleston, D. S.; Hwang, S. M.; Kline, T. P.; Koster, P. F.; Nichols, A.; Powers, D.; Romoff, T.; Samanen, J. M.; Stadel, J.; Vasko, J.; Kopple, K. D. Investigation of conformational specificity at GPIIb/IIIa: evaluation of conformationally constrained RGD peptides. *J. Med. Chem.* **1992**, *35*, 3962−3969. (e) Pfaff, M.; Tangemann, K.; Müller, B.; Gurrath, M.; Müller, G.; Kessler, H.; Timpl, R.; Engel, J. Selective recognition of cyclic RGD peptides of NMR defined conformation by $\alpha IIb\beta 3$, $\alpha v\beta 3$ and $\alpha 5\beta 1$ integrins. *J. Biol. Chem.* **1994**, *269*, 20233−20238. (f) Müller, G.; Gurrath, M.; Kessler, H. Pharmacophore refinement of gpIIb/IIa antagonists based on comparitive studies of antiadhesive cyclic and acyclic RGD peptides. *J. Comput.-Aided Mol. Des.* **1994**, *8*, 709−730. (g) Haubner, R.; Finsinger, D.; Kessler, H. Stereoisomeric Peptide Libraries and Peptidomimetics for Designing Selective Inhibitors of the $\alpha v\beta 3$ Integrin for a New Cancer Therapy. *Angew. Chem., Int. Ed.* **1997**, *36*, 1374−1389. (h) Duggan, M. E.; Duong, L. T.; Fisher, J. E.; Hamill, T. G.; Hoffman, W. F.; Huff, J. R.; Ihle, N. C.; Leu, C.-T.; Nagy, R. M.; Perkins, J. J.; Rodan, S. B.; Wesolowski, G. A.; Whitman, D. B.; Zartman, A. E.; Rodan, G. A.; Hartman, G. D. Nonpeptide $\alpha v\beta 3$ Antagonists. 1. Transformation of a Potent, Integrin-Selective $\alpha IIb\beta 3$ Antagonist into a Potent $\alpha v\beta 3$ Antagonist. *J. Med. Chem.* **2000**, *43*, 3736−3745.

(13) (a) Haubner, R.; Schmitt, W.; Hölzemann, G.; Goodman, S. L.; Jonczyk, A.; Kessler, H. Cyclic RGD Peptides Containing $\beta$-Turn Mimetics. *J. Am. Chem. Soc.* **1996**, *118*, 7881−7891. (b) Pitts, W. J.; Wityak, J.; Smallheer, J. M.; Tobin, A. E.; Jetter, J. W.; Buynitsky, J. S.; Harlow, P. P.; Solomon, K. A.; Corjay, M. H.; Mousa, S. A.; Wexler, R. R.; Jadhav, P. K. Isoxazolines as Potent Antagonists of the Integrin $\alpha v\beta 3$. *J. Med. Chem.* **2000**, *43*, 27−40. (c) Batt, D. G.; Petraitis, J. J.; Houghton, G. C.; Modi, D. P.; Cain, G. A.; Coryay, M. H.; Mousa, S. A.; Bouchard, P. J.; Forsythe, M. S.; Harlow, P. P.; Barbera, F. A.; Spitz, S. M.; Wexler, R. R.; Jadav, P. K.; Disubstituted indazoles as potent antagonists of the integrin $\alpha v\beta 3$. *J. Med. Chem.* **2000**, *43*, 41−58. (d) Belvisi, L.; Bernardi, A.; Checchia, A.; Manzoni, L.; Potenza, D.; Scolastico, C.; Castorina, M.; Cupelli, A.; Giannini, G.; Carminati, P.; Pisano, C. Potent integrin antagonists from a small library of RGD-including cyclic pseudopeptides. *Org. Lett.* **2001**, *3*, 1001−1004. (e) Hölzemann, G. Recent advances in avb3 integrin inhibitors. *Drugs* **2001**, *4*, 72−81. (f) Sulyok, G. A. G.; Gibson, C.; Goodman, S. L.; Hölzemann, G.; Wiesner, M.; Kessler, H. Solid-Phase Synthesis of a Nonpeptidic RGD Mimetic Library: New Selective $\alpha v\beta 3$ Integrin Antagonists. *J. Med. Chem.* **2001**, *44*, 1938−1950. (g) Goodman, S. L.; Hölzemann, G.; Sulyok, G. A. G.; Kessler, H. Nanomolar Small Molecule Inhibitors for $\alpha v\beta 6$, $\alpha v\beta 5$, and $\alpha v\beta 3$ Integrins. *J. Med. Chem.* **2002**, *45*, 1045−1051.

(14) Lin, E. C. K.; Ratnikov, B. I.; Tsai, P. M.; Carron, C. P.; Myers, D. M.; Barbas, C. F., III; Smith, J. W. Identification of a region in the integrin $\beta 3$ subunit that conferes ligand binding specificity. *J. Biol. Chem.* **1997**, *38*, 23912−23920.

(15) Takagi, J.; Tetsuji, K.; Meredith, J.; Puzon-McLaughlin, W.; Takada, Y.; Changing ligand specificities of $\alpha v\beta 1$ and $\alpha v\beta 3$ integrins by swapping a short diverse sequence of a $\beta$ subunit. *J. Biol. Chem.* **1997**, *32*, 19794−19800.

(16) Xiong, J.-P.; Stehle, T.; Zhang, R.; Joachimiak, A.; Frech, M.; Goodman, S. L.; Arnaout, M. A. Crystal Structure of the Extracellular Segment of Integrin $\alpha v\beta 3$ in Complex with an Arg-Gly-Asp Ligand. *Science* **2002**, *296*, 151−155.

(17) Xiong, J.-P.; Stehle, T.; Diefenbach, B.; Zhang, R.; Dunker, R.; Scott, D. L.; Joachimiak, A.; Goodman, S. L.; Arnaout, M. A. Crystal Structure of the Extracellular Segment of Integrin $\alpha v\beta 3$. *Science* **2001**, *294*, 339−345.

(18) (a) Liddington, R. C.; and Ginsberg, M. H. Integrin activation takes shape. *J. Cell Biol.* **2002**, *158*, 833−839. (b) Takagi, J.; and Springer, T. A. Integrin activation and structural rearrangement. *Immunol. Rev.* **2002**, *186*, 141−163. (c) Arnaout, M. A. Integrin structure: new twists and turns in dynamic cell adhesion. *Immunol. Rev.* **2002** *186*, 125−140. (c) Humphries, M. J.; Symonds, E. J. H.; Mould A. P. Mapping functional residues onto integrin crystal structures. *Curr. Opin. Struct. Biol.* **2003**, *13*, 236−243.

(19) (a) Springer, T. A. Predicted and experimental structures of integrins and $\beta$-propellers. *Curr. Opin. Struct. Biol.* **2002**, *12*, 802−813. (b) Vinogradova, O.; Velyvis, A.; Velyviene, A.; Hu, B.; Haas, T. A.; Plow, E. F.; Qin, J. A structural mechanism of integrin $\alpha IIb\beta 3$ "inside-out" activation as regulated by its cytoplasmic face. *Cell* **2002**, *110*, 587−597. (c) Gottschalk, K.-E.; Adams, P. D.; Brunger, A. T.; Kessler, H. Transmembrane signal transduction of the $\alpha IIb\beta 3$ integrin. *Protein Sci.* **2002**, *11*, 1800−1812. (d) Adair, B. D.; Yeager, M. Three-dimensional model of the human platelet integrin $\alpha IIb\beta 3$ based on electron cryomicroscopy and X-ray crystallography. *PNAS*, **2002**, *99*, 14059−14064. (e) Takagi, J.; Strokovich, K.; Springer, T. A.; Walz, T. Structure of integrin $\alpha 5\beta 1$ in complex with fibronectin. *EMBO J.* **2003**, *22*, 4607−4615. (f) Gottschalk, K.-E.; Kessler, H. Evidence for Hetero-Association of Transmembrane helices of Integrins. *FEBS Lett.* **2004**, *557*, 253−258.

(20) (a) Gottschalk, K.-E.; Günther, R.; Kessler, H. A Three-State Mechanism of Integrin Activation and Signal Transduction for Integrin $\alpha v\beta 3$. *ChemBioChem* **2002**, *3*, 470−473. (b) Gottschalk, K.-E.; Kessler, H. The Structures of Integrins and Integrin-Ligand Complexes: Implications for Drug Design and Signal Transduction. *Angew. Chem., Int. Ed.* **2002**, *41*, 3767−3774. (c) Marinelli, L.; Lavecchia, A.; Gottschalk, K. E.; Novellino, E.; Kessler, H. Docking studies on $\alpha v\beta 3$ Integrin Ligands: Pharmacophore Refinement and Implication for Drug Design. *J. Med. Chem.* **2003**, *46*, 4393−4404.

(21) (a) You, T. J.; Maxwell, D. S.; Kogan, T. P.; Chen, Q.; Li, J.; Kassir, J.; Holland, G. W.; Dixon, R. A. F. A 3D Structure Model of Integrin $\alpha 4\beta 1$ Complex: Construction of a Homology Model of $\beta 1$ and Ligand Binding Analysis. *Biophys J.* **2002**, *82*, 447−457. (b) Feuston, B. P.; Culberson, J. C.; Duggan, M. E.; Hartman, G. D.; Leu, C.-T.; Rodan, S. B. Binding Model for Nonpeptide Antagonists of $\alpha_v\beta_3$ Integrin. *J. Med. Chem.* **2002**, *45*, 5640−5648. (c) Feuston, B. P.; Culberson, J. C.; Hartman, G. D. Molecular Model of the $\alpha IIb\beta 3$ Integrin. *J. Med. Chem.* **2003**, *46*, 5316−5325.

(22) Plow, E. F.; Haas, T. A.; Zhang, L.; Loftus, J.; Smith J. W. Ligand binding to integrins. *J. Biol. Chem.* **2000**, *275*, 21785−8.

(23) (a) Masumoto, A.; Hemler, M. E. Mutation of putative divalent cation sites in the a4 subunit of the integrin VLA-4: Distinct effects on adhesion to CS1/fibronectin, VCAM-1, and invasin. *J Cell Biol* **1993**, *123*, 245−53. (b) Wilcox, D. A.; Paddock, C. M.; Lyman, S.; Gill, J. C.; Newman, P. J. Glanzmann thrombasthenia resulting from a single amino acid substitution between the second and third calcium-binding domains of GPIIb. Role of the GPIIb amino terminus in integrin subunit association. *J. Clin. Invest.* **1995**, *95*, 1553−60. (c) Mitchell, W. B.; Li, J.; Singh, F.; Michelson, A. D.; Bussel, J.; Coller, B. S.; French, D. L. Two novel mutations in the {alpha}IIb calcium-binding domains identify hydrophobic regions essential for {alpha}IIb-{beta}3 biogenesis. *Blood* **2003**, *101*, 2268−76.

(24) Takagi, J.; DeBottis, D. P.; Erickson, H. P.; Springer, T. A. The role of the specificity-determining loop of integrin $\beta$ subunit I-like domain in autonomous expression, association with the $\alpha$ subunit, and ligand binding. *Biochemistry* **2002**, *41*, 4339−4347.

(25) Miller, W. H.; Keenan, R. M.; Willette, R. N.; Lark, M. W. Identification and *in vivo* efficacy of small-molecule antagonist of integrin $\alpha v\beta 3$ (the vitronectin receptor). *Ther. Focus.* **2000**, *5*, 397−408.

(26) Arnaout, M. A.; Goodman, S. L.; Xiong, J. P. Coming to grips with integrin binding to ligands. *Curr. Opin. Cell. Biol.* **2002**, *14*, 641−651.

(27) Yamanouchi, J.; Hato, T.; Tamura, T.; Fujita, S. Identification of critical residues for ligand binding in the integrin beta3 I-domain by site-directed mutagenesis. *Thromb. Haemost.* **2002**, *87*, 756−762.

(28) Yahalom, D.; Wittelsberger, A.; Mierke, D. F.; Rosenblatt, M.; Alexander, J. M.; Chorev, M. Identification of the Principal Binding Site for RGD-Containing Ligands in the αvβ3 Integrin: A Photoaffinity Cross-Linking Study. *Biochemistry* **2002**, *41*, 8321−8331.
(29) Honda, S.; Tomiyama, Y.; Pampori, N.; Kashiwagi, H.; Kiyoi, T. Kosugi, S.; Tadokoro, S.; Kurata, Y.; Shattil, S. J.; Matsuzawa, Y. Ligand binding to integrin αvβ3 requires tyrosine 178 in the αv subunit. *Blood* **2001**, *97*, 175−182.
(30) (a) Metzger, T. G.; Paterlini, M. G., Portoghese, P. S.; Ferguson, D. M. Application of the message-address concept to the docking of naltrexone and selective naltrexone-derived opioid antagonists into opioid receptors models. *Neurochem. Res.* **1996**, *21*, 1287−1294. (b) Simpson, M. M.; Ballesteros, J. A.; Chiappa, V.; Chen, J.; Suehiro, M.; Hartman, D. S.; Godel, T.; Snyder, L. A.; Sakmar, T. P.; Javitch, J. A. Dopamine D4/D2 receptor selectivity is determined by a divergent aromatic microdomain contained within the second, third, and seventh membrane-spanning segments. *Mol. Pharmacol.* **1999**, *56*,1116−1126. *(*c) Paterlini, M. G. Structure Modeling of the Chemochine Receptor CCR5: Implications for Ligand Binding and Selectivity.
(31) Thompson, J. D.; Higgins, D. G.; Gibson, T. J. Improving the sensitivity of progressive multiple sequence alignment through sequence weighting, position-specific gap penalties and weight matrix choice. *Nucleic Acids Res.* **1994**, *22*, 4673−4680.
(32) Sali, A.; Potterton, L.; Yuan, F.; van Vlijmen, H.; Karplus, M. Evaluation of Comparative modeling by MODELLER. *Protein* **1995**, *23*, 318−326.
(33) Pedretti, A.; Villa, L.; Vistoli, G. VEGA: a Versatile Program to Convert, Handle, and Visualize Molecular Structure on Windows-based PCs. *J. Mol. Graph.* **2002**, *21*, 47−49.
(34) Accelrys, 2001, San Diego, CA.
(35) Laskowski, R. A.; MacArthur, M. W.; Moss, D. S.; Thornton, J. M. PROCHECK: a Program to Check the Stereochemical Quality of Protein Structures. *J. Appl. Crystallogr.* **1993**, *26*, 283−291.
(36) Morris, G. M.; Goodsell, D. S.; Halliday, R. S.; Huey, R.; Hart, W. E.; Belew, R. K.; Olson, A. J. Automated docking using a Lamarckian genetic algorithm and an empirical binding free energy function. *J. Comput. Chem.* **1998**, *19*, 1639−1662.
(37) SYBYL Molecular Modeling System (version 6.8), TRIPOS Assoc., St. Louis, MO.
(38) Head, J.; Zerner, M. C. A Broyden-Fletcher-Goldfarb-Shanno Optimization Procedure for Molecular Geometries. *Chem. Phys. Lett.* **1985**, *122*, 264−274.
(39) Vinter, J. G.; Davis, A.; Saunders: M. R. Strategic Approaches to Drug Design. 1. An Integrated Software Framework for Molecular Modelling. *J. Comput.-Aided Mol. Des.* **1987**, *1*, 31−55.
(40) Gasteiger, J.; Marsili, M. Iterative partial equalization of orbital electronegativity − a rapid access to atomic charges. *Tetrahedron* **1980**, *36*, 3219−3228.
(41) Allen, F. H.; Bellard, S.; Brice, M. D.; Cartwright, B. A.; Doubleday: A.; Higgs, H.; Hummelink, T.; Hummelink-Peters, B. G.; Kennard, O.; Motherwell, W. D. S. The Cambridge Crystallographic Data Center: Computer-Based Search, Retrieval, Analysis and Display of Information. *Acta Crystallogr.* **1979**, *B35*, 2331−2339.
(42) (a) Chakravorty, S.; Reynolds, C. H. Improved AMBER torsional parameters for the N−N rotational barrier in diacylhydrazines. *J. Mol. Graph. Model.* **1999**, *17*, 315−324. (b) Günther, R.; Hofmann, H. J. Hydrazino peptides as foldamers: an extension of the β-peptide concept. *J. Am. Chem. Soc.* **2001**, *123*, 247−255.

JM030635J